Supporting Information for: Dynamics in Polyelectrolyte/Microemulsion Complexes

Miriam Simon* and Michael Gradzielski†

Stranski-Laboratorium für Physikalische und Theoretische Chemie, Institut für Chemie, Technische Universität Berlin, Straße des 17. Juni 124, Sekr. TC 7, D-10623 Berlin, Germany

Ingo Hoffmann‡

Institut Max von Laue-Paul Langevin (ILL), 71 avenue des Martyrs, CS 20156, F-38042 Grenoble Cedex 9, France

(Dated: 2020-07-30)

VISCOSITY MEASUREMENTS

The viscosity of samples was measured using a micro-Ostwald capillary at 25.0 ± 0.1 °C. The addition of the microemulsion to the polyelectrolytes results in a slight decrease of the viscosity but all samples show very low values and are essentially water like (see fig. S1).

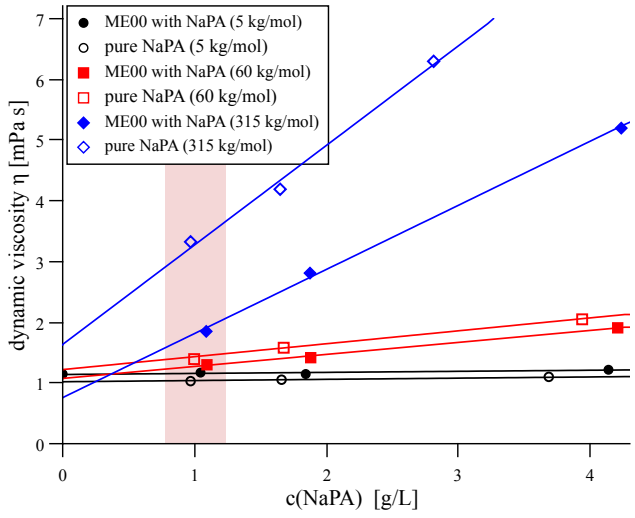

FIG. S1. Viscosity of polyelectrolyte/microemulsion complexes for different Mw of NaPA and different amounts of added polyelectrolyte. The red shaded area is marking the samples at a charge ratio of $z = 0.7$ used in this work.

DLS MEASUREMENTS

Dynamic light scattering (DLS) measures the intensity autocorrelation function $g^{(2)}$, which is related to the field autocorrelation function $g^{(1)}$ through the Siegert relation: $g^{(2)} = B\left|g^{(1)}\right|^2 + 1$, where B is an experimental prefactor. Correlation functions were recorded for detector angles between 40° and 130° and $g^{(1)}(t)$ of each angle was fitted with a stretched exponential function $g^{(1)}(t) = A \cdot \exp\left(-(t/\tau)^{\alpha}\right)$ to obtain the decay time τ. The stretched exponential function can be interpreted as superposition of simple exponentials with a distribution of relaxation times and we use it here to account for (small) polydispersity effects. The nth moment of the distribution is given by $< \tau^n >= \frac{\tau^n}{\alpha} \cdot \Gamma\left(\frac{n}{\alpha}\right)$, so that the average relaxation time is $\tau_{av} = \frac{\tau}{\alpha} \cdot \Gamma\left(\frac{1}{\alpha}\right)$ and Γ is the gamma function. Finally, the collective diffusion coefficient D can be calculated by $D = \frac{1}{\tau_{av} q^2}$ with the modulus of the

scattering vector (q), defined as: $q = (4\pi n_0 \cdot \sin(\theta/2))/\lambda$ where n_0 is the refractive index of the solution and θ the scattering angle and values were averaged over all q. Measurements were performed on an ALV/CGS-3 instrument, with a HeNe laser with a wavelength of $\lambda = 632.8$ nm. Pseudo-cross-correlation functions were recorded using an ALV 5000/E multiple-τ correlator at scattering angles θ ranging from 40° to 130° set with an ALV-SP 125 goniometer.

EXAMPLES OF NSE AND DLS CURVES

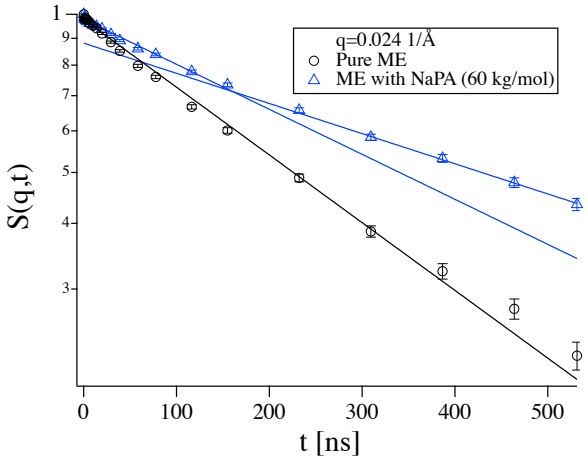

FIG. S2. Normalised intermediate scattering function for the pure microemulsion and the complex at $z = 0.7$ using NaPA with $M_w = 60$ kg/mol for the same q. While the pure microemulsion can be described with a single exponential, the complex clearly shows deviations from single exponential behaviour, indicating the presence of a second slower mode. The discrepancy in initial slope is due to the structure factor $S(q) < 1$ for the pure microemulsion at the q shown leading to a faster decay, lines are a guide to the eye.

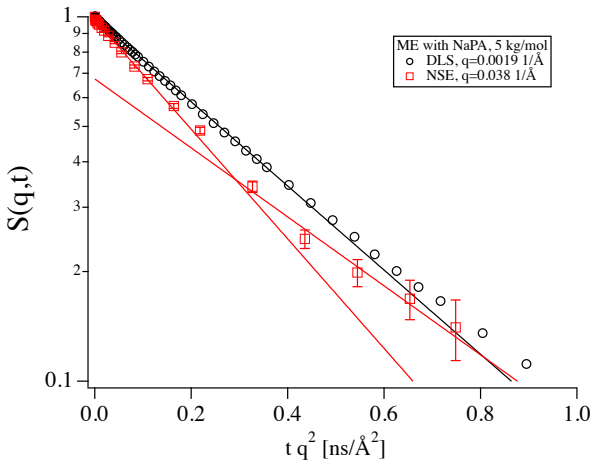

FIG. S3. Normalised intermediate scattering function for the complex at $z = 0.7$ using NaPA with $M_w = 5.1$ kg/mol, measured by DLS and NSE. While the DLS data can be described with a single exponential, the NSE data clearly shows deviations from single exponential behaviour, indicating the presence of a second slower mode, lines are a guide to the eye.

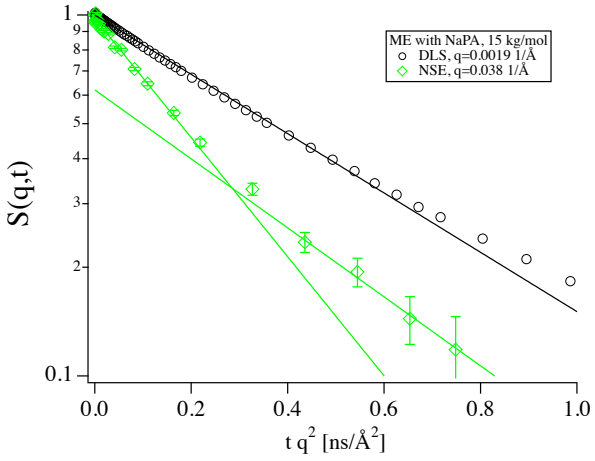

FIG. S4. Normalised intermediate scattering function for the complex at $z = 0.7$ using NaPA with $M_w = 15$ kg/mol, measured by DLS and NSE. While the DLS data can be described with a single exponential, the NSE data clearly shows deviations from single exponential behaviour, indicating the presence of a second slower mode, lines are a guide to the eye.

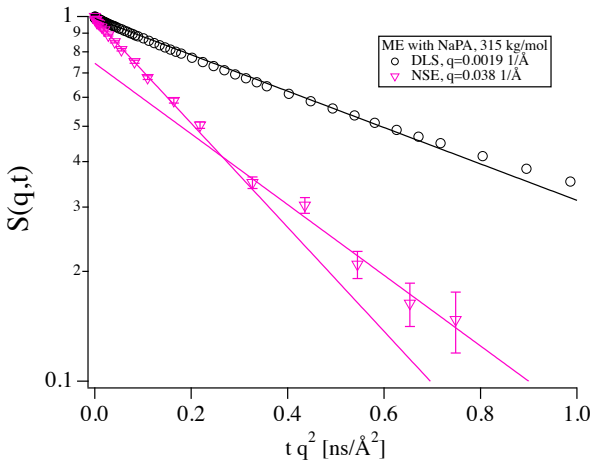

FIG. S5. Normalised intermediate scattering function for the complex at $z = 0.7$ using NaPA with $M_w = 315$ kg/mol, measured by DLS and NSE. While the DLS data can be described with a single exponential, the NSE data clearly shows deviations from single exponential behaviour, indicating the presence of a second slower mode, lines are a guide to the eye.

MODELING THE NSE DATA

Neutron spin-echo (NSE) measurements were performed on the instrument IN15 [1, 2] at Institut Laue Langevin (ILL, Grenoble, France) using wavelengths of 6, 10 and 14 Å reaching Fourier times of 42, 194 and 531 ns and covering a q range from 0.019 to 0.14 1/Å. Standard methods were applied for data reduction.

In addition to simple translational motion, microemulsion droplets also show membrane undulations which can be observed using NSE[3]. Their behaviour can be described using the Milner-Safran model[4, 5]. As they have a very low interfacial tension their dynamics are governed by their bending elasticity, which can be described with the Helfrich bending Hamiltonian[6]:

$$E = \int \left\{ (c_1 + c_2 - 2c_0)^2 \kappa/2 + \bar{\kappa} c_1 c_2 \right\} \mathrm{d}A + {}^1N k_B T \Phi(\phi), \tag{S1}$$

where κ is the mean bending modulus, $\bar{\kappa}$ the Gaussian modulus, c_0 the spontaneous curvature, c_1 and c_2 are the principal curvatures, A is the total surface of the system and ${}^1N$ is the particle number density of the droplets. In the random mixing approximation, the entropy term Φ is given by

$$\Phi(\phi) = \frac{1}{\phi} \left(\phi \ln(\phi) + (1-\phi) \ln(1-\phi) \right), \tag{S2}$$

where ϕ is the volume fraction of the droplet phase.

The form factor of a sphere is expanded it in terms of spherical harmonics, which, including the corrections from Farago and Gradzielski 3, results in the following expression:

$$\begin{aligned} P(q,R) &= P_{stat}(q,R) + P_{stat,corr}(q,R) + P_{dyn}(q,R) \\ P_{stat}(q,R) &= \left(\frac{4\pi R^2}{q} j_1(qR) \right)^2 \\ P_{stat,corr}(q,R) &= \frac{(4\pi)^2 R^2 j_1(qR)}{q} (2R j_0(qR) - qR^2 j_1(qR)) \\ &\quad \times \sum_{m \geq 2} \frac{2m+1}{4\pi} < a_m^2 > \\ P_{dyn}(q,R,t) &= (4\pi)^2 R^4 \sum_{m \geq 2} \frac{2m+1}{4\pi} j_m^2(qR) < a_m(0) a_m(t) >, \end{aligned} \tag{S3}$$

where R is the radius of the sphere. The j_m are the mth order spherical Bessel functions. P_{stat} simply corresponds to the form factor of a sphere, P_{dyn} is the dynamic part and $P_{stat,corr}$ is a correction to the static scattering similar to the Debye Waller factor. The sums in $P_{stat,corr}$ and P_{dyn} start from 2 as $m = 0$ corresponds to size fluctuations, which are too slow for the NSE timescale and $m = 1$ corresponds to translational motion, which is taken into account separately. The correlator $< a_m(0)a_m(t) >$ is given by $< a_m(0)a_m(t) >=< a_m^2 > \exp(-\Gamma_m t)$, where

$$< a_m^2 >= R^2 \times \frac{k_B T}{\kappa(m+2)(m-1)\left(m(m+1) - 6 + 4w - \frac{3\bar{\kappa}}{\kappa} - \frac{3k_B T}{4\pi\kappa}\Phi(\phi)\right)}$$

and

$$\Gamma_m = \frac{\kappa}{\eta R^3} \frac{m(m+1) - 6 + 4w - 3\bar{\kappa}/\kappa - \frac{3k_B T \Phi(\phi)}{4\pi\kappa}}{Z(m)} \tag{S4}$$

with $w = c_o R$. $Z(m)$ is a hydrodynamic factor given by

$$Z(m) = \frac{(2m+1)(2m^2+2m-1)}{m(m+1)(m+2)(m-1)}. \tag{S5}$$

To fit the data, only the $m = 2$ term is used for the undulation motion of the membrane, as the contributions from higher order terms are negligible and the contribution from the undulation motion is mostly seen around the form factor minimum.

The polydispersity of the microemulsion droplets is related to the bending modulus by

$$p^2 = \frac{\sigma^2}{R^2} = \frac{k_B T}{8\pi(2\kappa + \bar{\kappa}) + 2k_B T \cdot \Phi(\phi)} \tag{S6}$$

σ^2 is the variance of the size distribution. Here, we used a Gaussian distribution for the distribution of radii $f_R(R)$ with mean value R_{ME}.

As the microemulsion droplets are charged, and their concentration is relatively high, it is necessary to take their interactions into account, which was done here using the structure factor for charged colloids in the random phase approximation (RPA) [7]. It splits the interactions into a contribution from an hard sphere reference fluid with radius R_{eff} and volume fraction ϕ_{eff} to account for strong repulsions at short distances and a perturbation term U_{eff}:

$$S_{BA}(q) = \frac{1}{1 - {}^1N C_{eff}(q) - {}^1N \frac{U_{eff}(q)}{k_B T}}. \tag{S7}$$

C_{eff} is the direct correlation function of the reference hard sphere fluid, in the Percus-Yevick approximation:

$$
\begin{aligned}
{}^1NC_{eff}(x) = \Big[& A(\sin(x) - x\cos(x)) + B\left(\left(\frac{2}{x^2} - 1\right) x\cos(x) + 2\sin(x) - \frac{2}{x}\right) \\
& - \frac{\phi_{eff} A}{2}\left(\frac{24}{(x)^3} + 4\left(1 - \frac{6}{x^2}\right)\sin(x) \; - \left(1 - \frac{12}{x^2} + \frac{24}{x^4}\right) x\cos(x)\right)\Big] \frac{1}{x^3}, \quad \text{(S8)}
\end{aligned}
$$

where $x = 2qR_{eff}$, $A = -24\phi_{eff}\frac{(1+2\phi_{eff})^2}{(1-\phi_{eff})^4}$, $B = 36\phi_{eff}^2\frac{(2+\phi_{eff})^2}{(1-\phi_{eff})^4}$.

The perturbation term is obtained by Fourier transformation of the DLVO potential and reads

$$
{}^1NU_{eff}(x) = 24\phi_{eff}\pi\epsilon 2R_{eff}\psi^2\frac{x\cos(x) + s\sin(x)}{x^3 + xs^2}, \quad \text{(S9)}
$$

where $s = 2R_{eff}\kappa_{DH}$ with the inverse Debye-Hückel screening length $\kappa_{DH} = \sqrt{\frac{2N_a e^2 I_{ion}}{\epsilon k_B T}}$, with dielectric constant ϵ, elementary charge e, ionic strength I_{ion}, Avogadro constant N_a and the effective surface potential

$$
\psi = \frac{le}{4\pi\epsilon R_{eff}(1 + \kappa_{DH}R_{eff})}, \quad \text{(S10)}
$$

where l is the number of charges per particle and we used $R_{eff} = R$ and $\phi_{eff} = \phi$ for our fits.

The effective translational diffusion coefficient of the system is affected by the structure factor through de Gennes narrowing [8] and the hydrodynamic function $H(q)$, such that it reads

$$
D_{eff}(q) = \frac{D_0 \cdot H(q)}{S(q)}, \quad \text{(S11)}
$$

where $H(q)$ is usually much smaller than $S(q)$ and can therefore be neglected. D_0 is the diffusion coefficient at infinite dilution, which is related to the hydrodynamic radius R_H by the Stokes-Einstein equation:

$$
D_0 = \frac{k_B T}{6\pi\eta R_H} \quad \text{(S12)}
$$

with the viscosity of the solvent η and for a sphere of radius R at infinite dilution $R = R_H$. At sufficiently high q ($q > q_{peak}$) $S(q) \approx 1$, where q_{peak} is the position of the structure factor peak, and the radius of the sphere is obtained again, even for interacting systems. The consequence of eq. (S11) for systems with repulsive interactions is that at low q D_{eff} is larger than D_0, making particles appear smaller and around the structure factor peak, D_{eff} is smaller than D_0 making particles appear bigger.

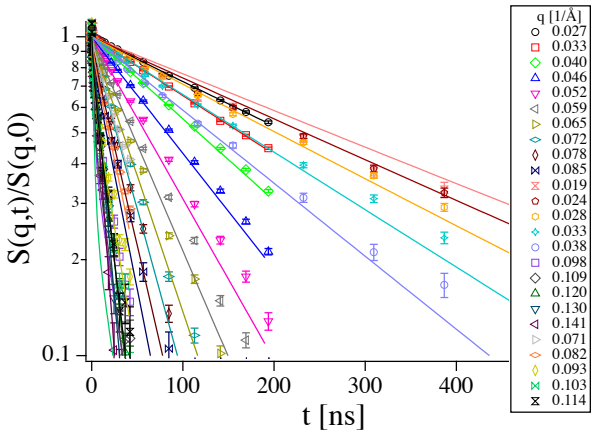

FIG. S6. Fits obtained for NSE data of the pure microemulsion using eq. (S13).

Combining eqs. (S2) to (S12) results in the following expression for the intermediate scattering function of charged microemulsions

$$s(q,t) = \int f_R(R)\left(P_{stat}(q,R) + P_{stat,corr}(q,R) + P_{dyn}(q,R,t)\right) \times \exp(-D_{eff}(q,R)q^2 t)\mathrm{d}R. \quad \text{(S13)}$$

In our fits (see fig. S6) we set $\kappa = \bar{\kappa}$ as the corrections from the Gaussian modulus are rather small, leaving R, κ and l as free parameters. From the fit we obtain κ=4.5 k_BT, $R = 43.2$ Å and $l = 8.4$ e. These values were used as constant input parameters for the fits of the PEMECs. For R and κ it is already evident from fig. 2 that no strong changes are observed as neither the q position of the peak due to the undulation motion changes nor its height relative to the level of D_{app} at lower q where only translational diffusion is observed.

For the PEMECs, a second slower mode was observed due to the diffusion of larger clusters in which microemulsion droplets are adsorbed on the polyelectrolyte. This behaviour was simply modelled by

$$s(q,t) = \int f_R(R)\left(P_{stat}(q,R) + P_{stat,corr}(q,R) + P_{dyn}(q,R,t)\right) \times \left(x_{slow}\exp(-D_{slow}q^2 t) + (1-x_{slow})\exp(-D_{eff}(q,R)q^2 t)\right)\mathrm{d}R \quad \text{(S14)}$$

with the slow diffusion coefficient D_{slow} and the fraction of intensity it accounts for x_{slow}. This means that we assume the bending undulations remain unaffected by the adsorption to the PE, which turned out to be a reasonably good approximation. However, the focus of this paper is on the diffusion of the complexes and the impact of the complex formation

on the bending rigidity will be investigated in detail in a future paper using microemulsions in film contrast where the effect of the bending motion is more clearly seen. For the fits of the data from PEMECs the same parameters as for the corresponding pure microemulsion were used, D_{slow} was a global q independend fit parameter and x_{slow} was treated as a free q dependent parameter.

We are using the local monodisperse approximation[9] for the incorporation of the structure factor, which has been successfully used for similar systems in the past [10–12].

Finally, the normalised intermediate scattering function is obtained by dividing $s(q,t)$ by $s(q,0)$:

$$S(q,t) = s(q,t)/s(q,0). \tag{S15}$$

Equation (S14) is a simplification as it considers only interactions between free microemulsion particles while in principle different partial structure factors between all the different components of the systems (free microemulsion droplets, complexes and droplets in complexes) would have to be taken into account. This is beyond the scope of this paper and it is most likely hopeless to try to obtain an expression that can be reasonably used to fit experimental data.

Here, we tried different approaches to tackle the problem. 1) First we tried to model the data leaving the structure factor obtained from fits to the data from the corresponding microemulsions unchanged (see fig. S7, top left). 2) Secondly, we treated the added polyelectrolyte as a simple electrolyte, which enters in S_{BA} through the screening length. This dampens the effect of the structure factor as it should also happen in practice through the addition of the polyelectrolyte. The polyelectrolyte adds its own counterions to the system, part of the charge of droplets that are bound to the polyelectrolyte are compensated and the structure factor peak for the larger complexes, if it is present at all, should be at a lower q value, which is not in the NSE q range. On the other hand, a peak from correlations between droplets inside a complex could appear. However, this is not seen in the data (see fig. 4). 3) We also tried to reduce the volume fraction used in the calculation of S_{BA} as in principle droplets bound in the complexes should not contribute to the structure factor of free droplets (see fig. S7, top right). It seems tempting to reduce ϕ for the structure factor to $\phi(1 - x_{slow})$. However it should be kept in mind that x_{slow} is an intensity fraction and not a volume fraction, even though they should be comparable at this q. Testing a rather extreme case, namely reducing the volume fraction to 10% of its nominal value allows us to

test, whether or not it has a significant influence on the outcome. 4) Lastly, we completely neglected the structure factor, setting $S_{BA} = 1$ (see fig. S7, bottom left).

It turned out, that the effect of the different treatments of interactions in the system has a rather small effect on the outcome, even more so since in a large part of the NSE q range ($q > 0.05$ 1/Å) $S(q)$ is close to 1. Other than an overly pronounced change of x_{slow} with q near the nominal structure factor peak and slightly different values for D_{slow} no effects are observed (see fig. S7, bottom right and fig. S8). The somewhat higher D_{slow} for the treatment with an unchanged structure factor seems reasonable as for the most part of the q range the value of $S_{BA} \geq 1$ resulting in apparently slower diffusion for the droplets themselves so that the correction for the additional slow contribution can be faster. Using a reduced volume fraction with or without additional screening has a similar but less pronounced effect as additional screening at the nominal volume fraction and we decided to fit our data treating the polyelectrolyte as simple electrolyte and leaving the volume fraction at its nominal value (approach 2). The obtained fits can be found in figs. S9 to S12.

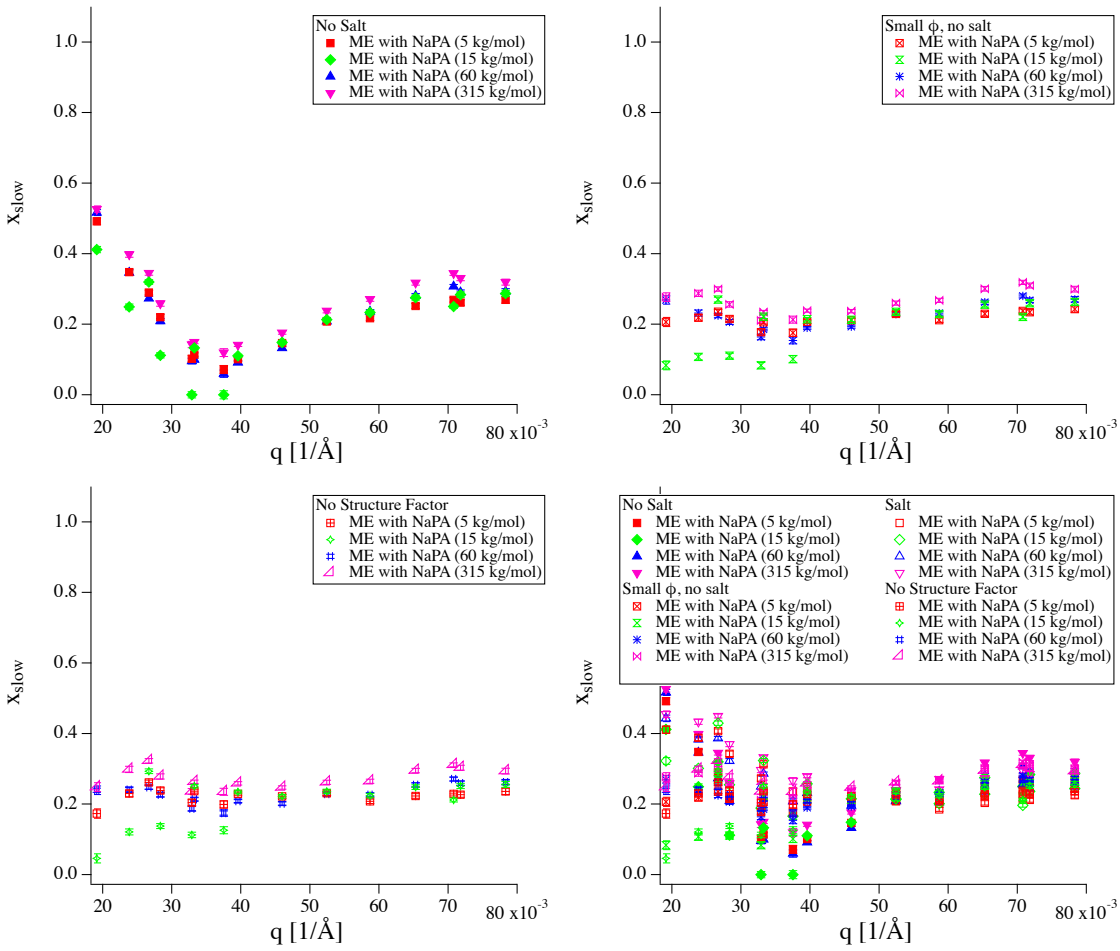

FIG. S7. Results obtained for x_{slow} from fitting data to eq. (S15) with eq. (S14) with different methods for taking into account the structure factor. Top left: Approach 1, leaving the structure factor from the pure MEs unchanged; Top right: Approach 3, structure factor with 10% nominal volume fraction; Bottom left: Approach 4, neglecting the structure factor. For better comparison all different approaches, including approach 2 (treating the polyelectrolyte as simple salt, shown in the main article, fig. 4) are shown together in the bottom right panel. No significant differences can be observed away from the structure factor peak.

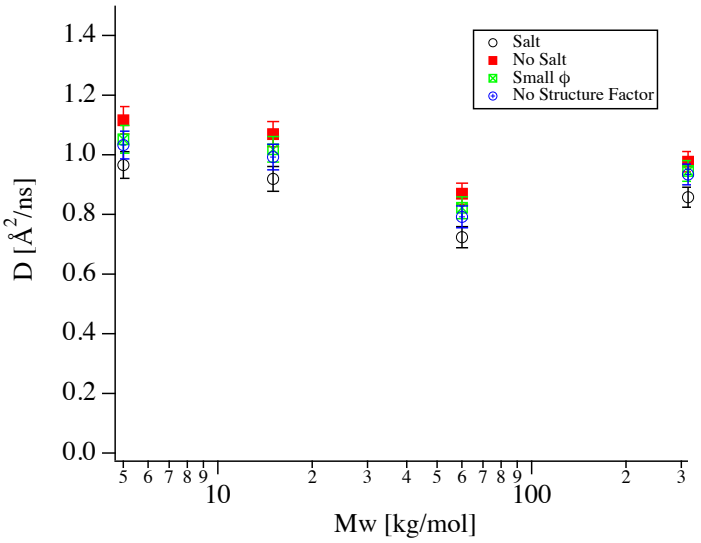

FIG. S8. Results obtained for D_{slow} from fitting data to eq. (S15) with eq. (S14) with different methods for taking into account the structure factor. The exact fitting methods has only a small influence on the result.

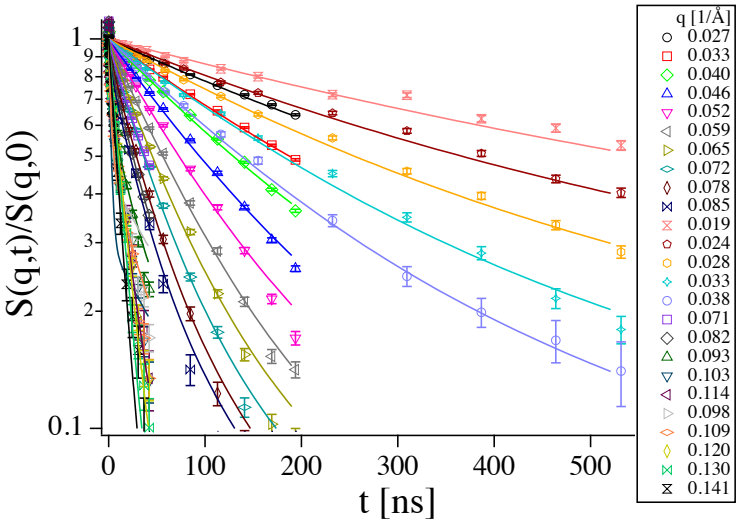

FIG. S9. Fits obtained for NSE data of microemulsion with NaPA with a M_w of 5 kg/mol using eq. (S15) with eq. (S14) and treating NaPA as simple salt (approach 2).

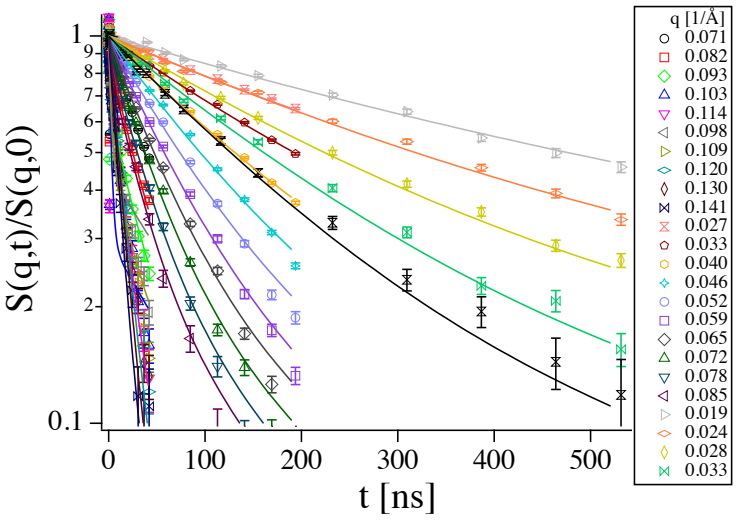

FIG. S10. Fits obtained for NSE data of microemulsion with NaPA with a M_w of 15 kg/mol using eq. (S15) with eq. (S14) and treating NaPA as simple salt (approach 2).

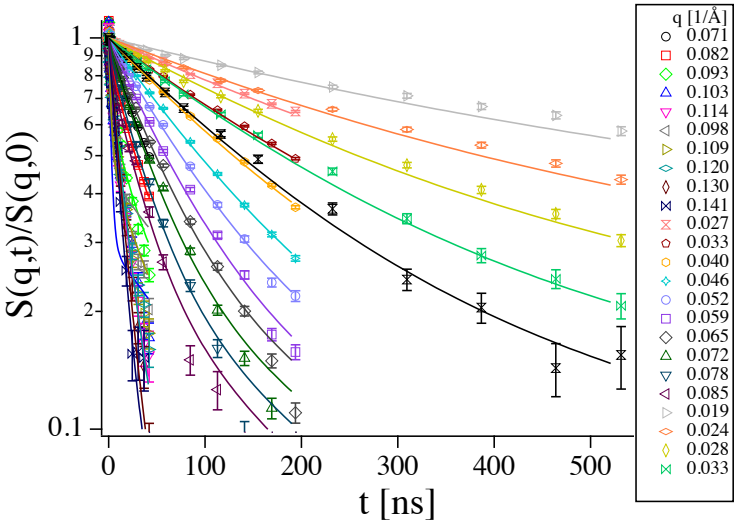

FIG. S11. Fits obtained for NSE data of microemulsion with NaPA with a M_w of 60 kg/mol using eq. (S15) with eq. (S14) and treating NaPA as simple salt (approach 2).

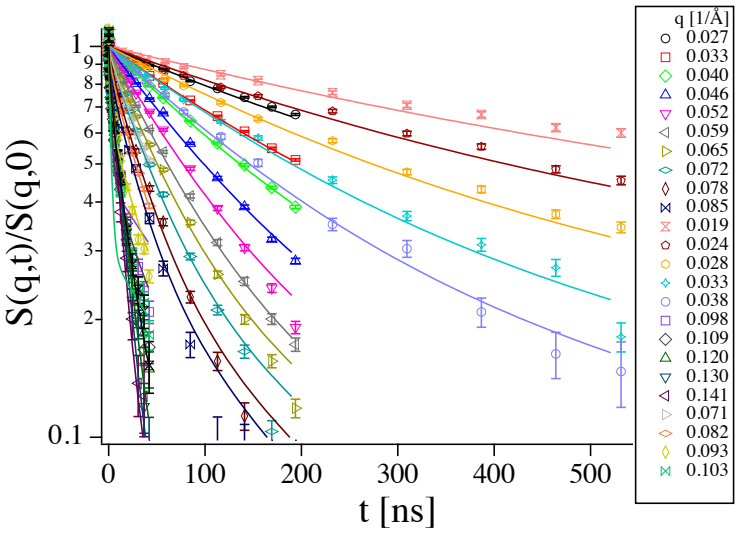

FIG. S12. Fits obtained for NSE data of microemulsion with NaPA with a M_w of 315 kg/mol using eq. (S15) with eq. (S14) and treating NaPA as simple salt (approach 2).

SMALL-ANGLE NEUTRON SCATTERING (SANS)

SANS Experiments

SANS experiments were carried out on PAXY at Laboratoire Lon Brillouin (LLB) in Saclay (three configurations: sample-to-detector distances of 1.2, 2, and 6 m, collimation lengths of 2, 2, and 6 m and wavelengths of 4, 10, and 10 Å, respectively, covering a q range from 0.0035 to 0.505 1/Å) and on V4 at Helmholtz-Zentrum Berlin (HZB) (three configurations: sample-to-detector distances of 1.35, 6.75, and 15.75 m, collimation lengths of 2, 8, and 16 m and wavelengths of 4.5, 4.5, and 10 Å, respectively, covering a q range from 0.0025 to 0.524 1/Å).

Data reduction was done using the software BerSANS [13]. The raw intensity data was corrected for the scattering of the background (solvent and sample container) and weighted by the transmission of the sample. Additionally, the (electronic) background noise was subtracted using a cadmium sample, which is absorbing all incoming neutrons. The normalisation and absolute scaling was done by using a 1 mm reference sample of deionised H_2O, as isotropic scatterer. Finally, the 2D data were radially averaged in 1D scattered intensity.

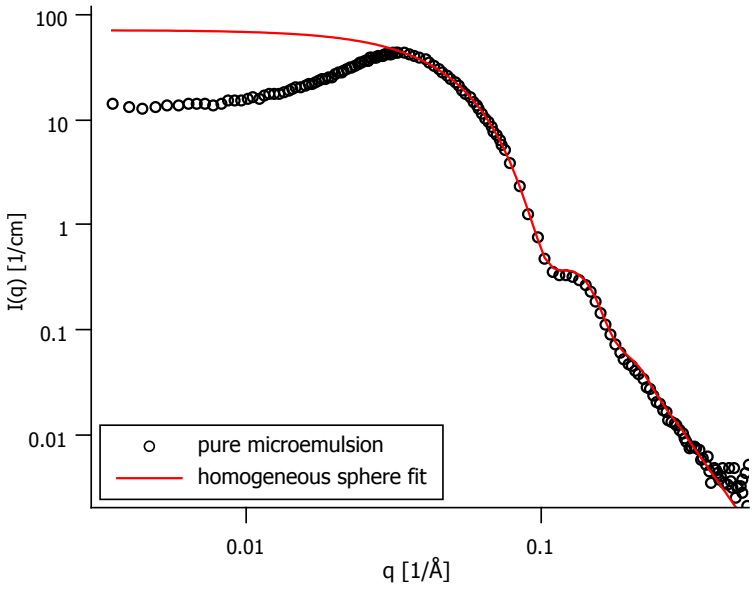

FIG. S13. SANS data of pure microemulsion showing the structure factor peak at about 0.04 1/Å.

Fitting Models

Fits were performed in absolute units and it was assumed that all of the surfactant, co-surfactant, and oil are contained in either the aggregates or the free microemulsion droplets. Due to the low concentration and its low contrast the polyelectrolyte was not considered explicitly for modelling of the data.

The shape of the scattering curve can be modeled as a combination of free, spherical microemulsion droplets and wormlike chains with contour length L and Kuhn length l_b. For the wormlike chain we use Kholodenko's formula [14]:

$$P'(q, L, l_b) = \frac{2}{x}\left(I_{(1)}(x) - \frac{1}{x}I_{(2)}(x)\right), \tag{S16}$$

defining $x = 3L/l_b$ and

$$I_{(n)}(x) = \int_0^x f(z) z^{n-1} \mathrm{d}z \tag{S17}$$

with

$$f(z) = \begin{cases} \frac{\sinh(Ez)}{E\sinh(z)} & \text{for } \frac{ql_b}{3} \leq 1 \\ \frac{\sin(Ez)}{E\sinh(z)} & \text{for } \frac{ql_b}{3} > 1 \end{cases} \tag{S18}$$

and

$$E = \sqrt{\left|1 - \left(\frac{ql_b}{3}\right)^2\right|}. \tag{S19}$$

This expression needs to be multiplied by another form factor to account for the cross sectional structure of the chains. Here, we simply assume a homogeneous, circular cross section:

$$P_{cs}(q, R) = \left(\frac{2J_1(q, R)}{qR}\right), \tag{S20}$$

with the first order Bessel function of the first kind J_1. To obtain absolute intensities, particle number density ${}^1N_w$, the difference in scattering length density ΔSLD and the volume of the wormlike chains $V_w = \pi R^2 L$ need to be taken into account:

$$I_w(q) = {}^1N_w(\Delta SLD)^2 \int f_{Rw}(R) V_w(R)^2 P'(q, L, l_b) P_{cs}(q, R) \mathrm{d}R, \tag{S21}$$

where ${}^1N_w = \frac{\phi_w}{\int f_{Rw}(R) V_w(R) \mathrm{d}R}$ and f_{Rw} is the distribution of radii in the wormlike chains with mean value R_w and ϕ_w is the volume fraction of wormlike chains which is related to the volume fraction of material in the sample ϕ by $\phi_w = \phi x_w$ and $0 \geq x_w \geq 1$.

Following the results from NSE we modelled the SANS data as a combination of eq. (S21), accounting for the slow mode and free microemulsion droplets. The static form factor of a spherical droplet is given by P_{stat} in eq. (S3) and we use the same structure factor as for the description of NSE data $S_{BA}(q)$ given in eq. (S7), so that the intensity of the microemulsion droplets reads

$$I_{ME}(q) = {}^1N_{ME}(\Delta SLD)^2 \int f_{RME}(R) P_{stat}(q,R) S_{BA}(q,R) \mathrm{d}R, \tag{S22}$$

where f_{RME} is the distribution of radii in the microemulsion droplets with the average droplet radius R_{ME} and the particle number density of the droplets is given by ${}^1N_{ME} = \frac{\phi_{ME}}{\int f_{RME}(R,R_{ME}) 4\pi/3 R^3 \mathrm{d}R}$ with the volume fraction of microemulsion droplets $\phi_{ME} = \phi(1-x_w)$ and the overall intensity is given by

$$I(q) = I_w(q) + I_{ME}(q). \tag{S23}$$

For the calculation of ϕ and ΔSLD all material except the PAA was considered as it is virtually invisible next to the strongly scattering microemulsion droplets. For the fits, x_w was fixed at 0.3 roughly in agreement with the results obtained from NSE and only L and l_b were left as free parameters, while all parameters in I_{ME} were left at the same values as for the NSE fits and the mean radius of the wormlike chains R_w was set to 34.5 Å to match the form factor minimum. For both distributions the relative standard deviation was set to 0.12 and a log normal size distribution was used. The fits are shown in fig. S14 and the fit parameters are summarised in table S I.

Discussion of the SANS Fit Results

Good fit results are obtained using eq. (S23) only around 0.02 1/Å some slight deviations are observed due to the oversimplified model of homogeneous wormlike chains. In reality they are inhomogeneous and consist of separate droplets which results in a lower intensity in this q range. For the same reason, we observe a radius of the wormlike chain R_w that is smaller than the microemulsion droplet radius R_{ME}, which leads to deviations around the form factor minimum at $q = 0.1$ 1/Å. In addition the implementation of the structure factor is an oversimplification as well. Nevertheless, this simple model captures the essential physics of the system and shows that the SANS data are compatible with our finding from

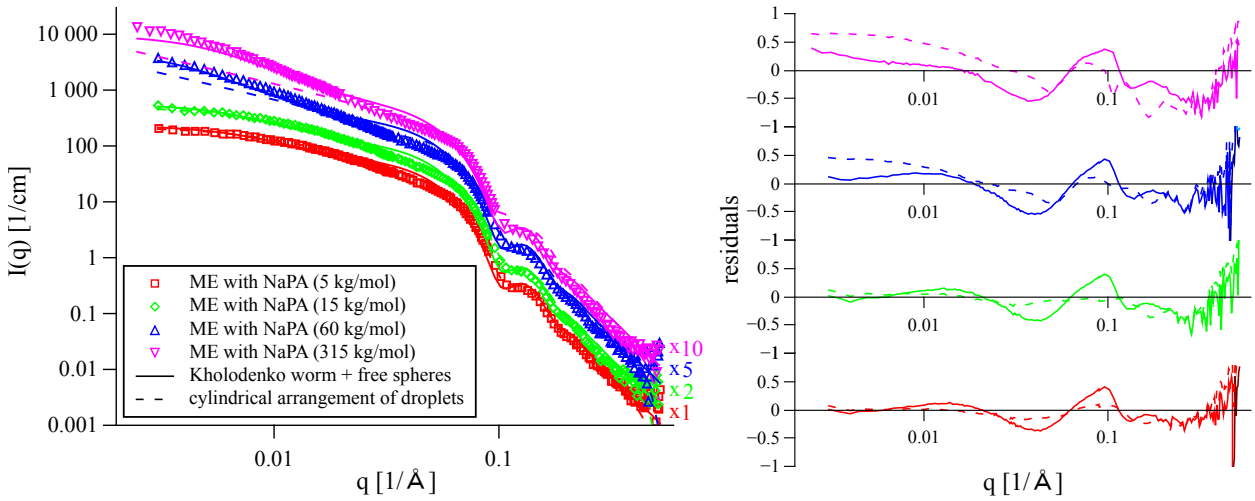

FIG. S14. SANS data of microemulsion with NaPA of different M_w. Fits and residuals are comparing the cylindrical arrangement of droplets model used in Simon *et al.* 15 (dotted lines) and the two components model of wormlike chains and free spheres (solid lines) that is consistent with the NSE results.

TABLE S I. Parameters of fits of eq. (S23) to SANS data shown in fig. 1. The fraction of wormlike chains x_w was kept at 0.3 according to NSE results and radii of microemulsion droplets and wormlike chains R_{ME} and R_w were used as global fit parameters. The contour length L and Kuhn length l_b were free fit parameters.

M_w [kg/mol]	R_{ME} [Å]	R_w [Å]	x_w	L [Å]	l_b [Å]
5.1	43.2	34.5	0.3	900	330
15	43.2	34.5	0.3	1100	290
60	43.2	34.5	0.3	4000	230
315	43.2	34.5	0.3	4000	130

NSE that only a relatively small fraction of the microemulsion droplets is adsorbed on the polyelectrolyte, even though this would not have been obvious from the SANS data.

Looking at the parameters in table S I it seems that the contour length of the aggregates greatly exceeds the contour length of the polyelectrolyte (∼140 Å for 5 kg/mol). There are at least two different explanations. The NaPAs used here are not particularly monodisperse and the scattering pattern might be dominated by some long chains present in the sample. On the other hand, this might also mean that the short lived aggregates do interconnect

multiple chains. Since no clear plateau at low q is reached in any of the SANS curves, some scepticism is advised regarding the precise values of L in general. The values of l_b are in reasonably good agreement with the values obtained for D_{slow} from NSE. Using the Stokes-Einstein equation (eq. (S12)) and a diffusion coefficient of 1 Å^2/ns (see fig. 5) a hydrodynamic radius of about 200 Å is obtained, which nicely corresponds to the values obtained for l_b and implies that the slow diffusion observed in NSE is related to the movement of segments of the aggregates. It is not quite clear if the decrease in l_b with the molecular weight of the NaPA is really due to the chain length or is just related to the slightly different treatment of the different NaPAs.

* miriam.simon@tu-berlin.de

† michael.gradzielski@tu-berlin.de

‡ hoffmann@ill.fr

[1] P. Schleger, B. Alefeld, J. Barthelemy, G. Ehlers, B. Farago, P. Giraud, C. Hayes, A. Kollmar, C. Lartigue, F. Mezei, and D. Richter, Phys. B **241–243**, 164 (1997).

[2] B. Farago, P. Falus, I. Hoffmann, M. Gradzielski, F. Thomas, and C. Gomez, Neutron News **26**, 15 (2015).

[3] B. Farago and M. Gradzielski, J. Chem. Phys. **114**, 10105 (2001).

[4] S. A. Safran, J. Chem. Phys. **78**, 2073 (1983).

[5] S. T. Milner and S. A. Safran, Phys. Rev. A **36**, 4371 (1987).

[6] W. Helfrich, Z. Naturforschung C **30**, 841 (1975).

[7] L. Baba-Ahmed, M. Benmouna, and M. J. Grimson, Phys. Chem. Liq. **16**, 235 (1987).

[8] P. G. De Gennes, Physica **25**, 825 (1959).

[9] J. S. Pedersen, J. Appl. Crystallogr. **27**, 595 (1994).

[10] I. Hoffmann, P. Malo De Molina, B. Farago, P. Falus, C. Herfurth, A. Laschewsky, and M. Gradzielski, J. Chem. Phys. **140**, 034902 (2014).

[11] T. Foster, T. Sottmann, R. Schweins, and R. Strey, J. Chem. Phys. **128**, 054502 (2008).

[12] T. Foster, T. Sottmann, R. Schweins, and R. Strey, J. Chem. Phys. **128**, 064902 (2008).

[13] U. Keiderling, Appl. Phys. A: Mater. Sci. Process. **74**, S1455 (2002).

[14] A. L. Kholodenko, Macromolecules **26**, 4179 (1993).

[15] M. Simon, P. Krause, L. Chiappisi, L. Noirez, and M. Gradzielski, Chem. Sci. **10**, 385 (2019).